

# Analytic solutions of the rise dynamics of liquid in a vertical cylindrical capillary

Xiaoxu Zhong<sup>a,1</sup>, Bohua Sun<sup>b,\*</sup>, Shijun Liao<sup>a,c,d,\*\*</sup>

<sup>a</sup> State Key Laboratory of Ocean Engineering, School of Naval Architecture, Ocean and Civil Engineering, Shanghai Jiao Tong University, Shanghai 200240, China

<sup>b</sup> School of Civil Engineering & Institute of Mechanics and Technology, Xi'an University of Architecture and Technology, Xi'an 710055, China

<sup>c</sup> State Key Laboratory of Plateau Ecology and Agriculture, Xining 810018, China

<sup>d</sup> School of Hydraulic and Electric Engineering, Qinghai University, Xining 810018, China

## ARTICLE INFO

### Article history:

Received 30 December 2018  
Received in revised form 12 May 2019  
Accepted 23 May 2019  
Available online 30 May 2019

### Keywords:

Capillary flow  
Vertical circular tube  
Homotopy analysis method

## ABSTRACT

Series solutions of the dynamics of capillary flows in a vertical circular tube are obtained by the homotopy analysis method (HAM). The model proposed by Maggi and Alonso-Marroquin (2012) is considered but with assumptions of constant contact angle and negligible air. In the case of capillary flows oscillating around the equilibrium height, the series solution of the penetration distance of the meniscus has the basis  $\exp(m\Re[\eta_1]\tau)\cos(n\Im[\eta_1]\tau)$  and  $\exp(m\Re[\eta_1]\tau)\sin(n\Im[\eta_1]\tau)$ . By contrast, in the case of capillary flows rising monotonically to the equilibrium height, the series solution of the penetration distance of the meniscus can have either the basis  $\exp[(m\eta_1 + n\eta_2)\tau]$ , if  $\eta_2/\eta_1 \neq \mathbb{Z}$ , or the basis  $\exp(m\eta_1\tau)$ . The computed velocity of the capillary flow is found to be larger than that of the experimental results. This discrepancy should be mainly caused by the neglect of both the variation of contact angle and the expulsion of air out of the capillary. Besides, the velocity of the capillary flow at the initial stage is determined by the Bond number and the viscosity effect becomes significant in the latter stage, which is consistent with the results of previous literature.

© 2019 Elsevier Masson SAS. All rights reserved.

## 1. Introduction

Capillary flow widely exists in nature, such as the flow transport in plants, soil, and pens. Many phenomena can be described (under certain assumptions) by the models of capillary flow in cylindrical tubes or porous materials [1–7]. The model characterizing rise dynamics of liquid in a vertical circular tube is as shown in Fig. 1, where  $r$  denotes the radius of the vertical circular tube,  $g$  is the acceleration due to gravity,  $\theta$  represents the dynamic contact angle between the meniscus and the wall of the tube,  $\sigma$  denotes the surface tension coefficient,  $h$  is the height of meniscus with respect to the outside static surface, respectively. The dynamic behavior of meniscus is primarily determined by the balance between the inertia of the fluid, the capillary driving

force, the weight of the liquid and the viscous resisting forces. The first comprehensive investigation of the capillary rise dynamics dates back to Bell and Cameron [8], Lucas [9] and Washburn [10], who considered the capillary flow in a cylindrical tube of radius  $r$  and presented the rate of penetration as

$$\frac{dh}{dt} = \frac{P(r^2 + 4\epsilon r)}{8\mu h}, \quad (1)$$

where  $t$  is the time for a liquid of dynamic viscosity  $\mu$  and slip coefficient  $\epsilon$  to penetrate a distance  $h$  into the capillary under the driven pressure  $P$ . However, in the initial stage, i.e.,  $t \rightarrow 0$ ,  $h \rightarrow 0$ ,  $dh/dt \rightarrow \infty$  can be derived from Eq. (1), this singularity does not coincide with reality. Since then, several nonlinear differential equations were presented based on different assumptions on the inertial force, entrance effect, and dynamic contact angle, etc.

Brittin [11] proposed a model by assuming the forces acting on the liquid in an accelerating state to be the same as that in a steady state

$$h \frac{d^2 h}{dt^2} + \frac{5}{4} \left( \frac{dh}{dt} \right)^2 + \frac{8\mu}{\rho r^2} h \frac{dh}{dt} - \frac{2\sigma \cos \theta}{\rho r} + gh = 0, \quad (2)$$

in which  $\rho$  denotes the density of the liquid. However,  $dh/dt \neq 0$  at initial moment ( $t \rightarrow 0$ ,  $h \rightarrow 0$ ), i.e., there also exists a singularity in this model.

\* Corresponding author at: School of Civil Engineering & Institute of Mechanics and Technology, Xi'an University of Architecture and Technology, Xi'an 710055, China.

\*\* Corresponding author at: State Key Laboratory of Ocean Engineering, School of Naval Architecture, Ocean and Civil Engineering, Shanghai Jiao Tong University, Shanghai 200240, China.

E-mail addresses: [sunbohua@xauat.edu.cn](mailto:sunbohua@xauat.edu.cn) (B. Sun), [sjliao@sjtu.edu.cn](mailto:sjliao@sjtu.edu.cn) (S. Liao).

<sup>1</sup> Present address: School of Mechanical Engineering, Purdue University, West Lafayette, IN 47906, United States.

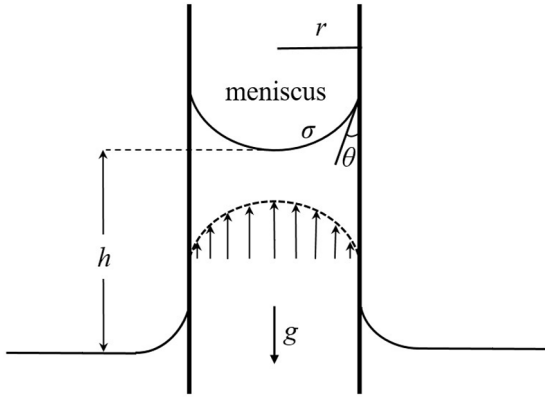


Fig. 1. Rise dynamics of a liquid in a vertical circular tube.

Szekely et al. [12] further took the energy dissipation into account and proposed a more rigorous equation that successfully removes the singularity

$$\left(h + \frac{7r}{6}\right) \frac{d^2h}{dt^2} + 1.225 \left(\frac{dh}{dt}\right)^2 + \frac{8\mu}{\rho r^2} h \frac{dh}{dt} - \frac{2\sigma \cos \theta}{\rho r} + gh = 0. \quad (3)$$

However, their treatment of dissipative effect refers to high Reynolds number, whereas most wetting phenomena in capillaries occur at low Reynolds number [13]. Levine et al. [13] further proposed an improved theory

$$\left(h + \frac{37r}{36}\right) \frac{d^2h}{dt^2} - \frac{2\sigma \cos \theta}{\rho r} + \frac{8\mu}{\rho r^2} h \frac{dh}{dt} + gh + \frac{1}{2} \left[ \frac{4\mu}{\rho r} \frac{dh}{dt} + \frac{7}{3} \left(\frac{dh}{dt}\right)^2 \right] = 0. \quad (4)$$

Subsequently, Xiao et al. [14] proposed a generalized model for capillary flows in channels. For the flow in a capillary tube, this model reads

$$(h + 1.028r) \frac{d^2h}{dt^2} + 0.958 \left(\frac{dh}{dt}\right)^2 + \frac{8\mu}{\rho r^2} (h + 0.25r) \frac{dh}{dt} - \frac{2\sigma \cos \theta}{\rho r} + gh = 0. \quad (5)$$

Maggi and Alonso-Marroquin [15] then considered the coupled effect of liquid–gas interactions and proposed following governing equations of two-phase flow in a capillary

$$2\pi r \sigma \cos \theta - \pi r^2 g L \rho(h) - 8\pi L \mu(h) \frac{dh}{dt} + W + \pi r^2 \Delta p = \pi r^2 L \rho(h) \frac{d^2h}{dt^2} \quad (6)$$

in which

$$L\rho(h) = \rho_l h + \rho_g(L - h), \quad L\mu(h) = \mu_l h + \mu_g(L - h) \quad (7)$$

$$W = \begin{cases} -\frac{\pi}{6} \rho_l r^2 \left(\frac{dh}{dt}\right)^2 & \text{when } \frac{dh}{dt} \geq 0, \\ \frac{\pi}{6} \rho_g r^2 \left(\frac{dh}{dt}\right)^2 & \text{when } \frac{dh}{dt} < 0, \end{cases} \quad (8)$$

$$\Delta p = \begin{cases} \rho_g g L - \frac{\rho_l - \rho_g}{2} \left(\frac{dh}{dt}\right)^2 - \frac{7}{6} \rho_l r \frac{d^2h}{dt^2} & \text{when } \frac{dh}{dt} \geq 0, \\ \rho_g g L - \frac{\rho_l - \rho_g}{2} \left(\frac{dh}{dt}\right)^2 - \frac{7}{6} \rho_g r \frac{d^2h}{dt^2} & \text{when } \frac{dh}{dt} < 0, \end{cases} \quad (9)$$

with  $L$  the length of the capillary tube,  $\rho_l$  and  $\rho_g$  the density of liquid and gas,  $\mu_l$  and  $\mu_g$  the liquid and gaseous dynamic viscosity, respectively. In addition, Maggi and Alonso-Marroquin [15] proved the robustness of model (6) by comparing numerical results with experimental data. Assuming that the contact angle  $\theta$  is constant and  $\rho_g = \mu_g = 0$ , Eq. (6) reduces to

$$(h + \varpi_1) \frac{d^2h}{dt^2} + \varpi \left(\frac{dh}{dt}\right)^2 + \frac{8\mu}{\rho r^2} h \frac{dh}{dt} - \frac{2\sigma \cos \theta}{\rho r} + gh = 0, \quad (10)$$

in which

$$\begin{cases} \varpi_1 = \frac{7}{6}r, & \varpi = \frac{2}{3} & \text{when } \frac{dh}{dt} \geq 0, \\ \varpi_1 = 0, & \varpi = \frac{1}{2} & \text{when } \frac{dh}{dt} < 0, \end{cases} \quad (11)$$

with  $\rho = \rho_l$  and  $\mu = \mu_l$ .

Researchers generally divide the process of liquid rising in a vertical cylindrical tube into several stages [16,17].  $h \propto t^2$  is derived by neglecting viscous and gravity terms at the first stage [16,18]. With viscous influence increases, the inertia dominated flow gradually evolves into the viscous flow. Detailed analysis of this transition can be found in the literature [16,17,19]. Subsequently, the effect of inertia vanishes and the flow becomes purely viscous,  $h \propto \sqrt{t}$  is derived by neglecting both inertia and gravity [9,10]. After that, the purely viscous flow enters into both the viscous and gravitational time stage. Analytic solutions in this stage (neglecting inertia) in implicit and explicit forms are given by Washburn [10] and Fries and Dreyer [20], respectively. In the end, the equilibrium height  $2\sigma \cos \theta / (\rho g r)$  where meniscus stops, which is also called the Jurin height [21], is determined by the balance of gravity and surface tension. It is worth mentioning that some oscillatory cases were noticed in experiments [16,22,23]. It is shown that the oscillation of meniscus position is mainly caused by kinetic force and it is the viscosity that mainly damps the oscillatory energy out. For a defined liquid and capillary tube, a critical value for capillary radius was suggested by Hamraoui and Nylander [24] and Masoodi et al. [25], below which the oscillation disappears. Besides, the imbibition dynamics depend on the shape of the free surface as well [26]. A universal law  $h \propto t^{1/3}$  is found when liquid rises into corners of different geometries [27] or into short pillars with rounded edges [28], but dynamics follows  $h \propto \sqrt{t}$  when liquid rises into long pillars with sharp edges [29]. Also, Siebold et al. [30] found that the contact angle depends strongly on the rising velocity.

Various experiments have been done to observe the behaviors of capillary action and to confirm the validity of theories. However, most of them, unfortunately, fail to cover the complete process. Early experiments [8,10,31] were performed under normal gravity condition with small tube diameter but only the  $h \propto \sqrt{t}$  behavior was observed. After that, Siegel [32] carried out free fall experiments in a low-gravity (including zero-gravity) environment with different tube diameters and successfully observed the  $h \propto t$  behavior. Subsequently, Dreyer et al. [18] performed a drop tower experiment, which verifies their theory that the capillary rise process is divided into three successive stages with at the beginning  $h \propto t^2$ , then  $h \propto t$ , and ultimately  $h \propto \sqrt{t}$ . These three regions later were verified by Stange et al. [16] who performed experiments under micro-gravity environment by using a 4.7 s drop tower. Moreover, Stange et al. [16] gave a detailed analysis of why many experiments could only observe parts of behavior. Stange et al. [16] proposed that the three phases of capillary rise process are separated by two characteristic time scales  $t_1 \propto \sqrt{\rho r^3 / \sigma}$  and  $t_2 \propto r^2 / \nu$  which are determined by Ohnesorge number  $Oh = \sqrt{\rho \nu^2 / (\sigma d)}$  and the inertia of the liquid.

To solve the established models as above, various numerical, such as the Runge–Kutta algorithm [17] and the Lattice-Boltzmann method [33], and analytical approaches [20,24] have been suggested and applied. Most commonly, numerical methods are recognized in the international research community on its availability and are accepted as the most convenient way of solving complex physical problems. However, it is difficult for researchers to draw physical intuition directly and to investigate the influence of physical parameters on processes from numerical solving steps, even though a numeric answer can be immediately obtained. So, obtaining analytic solutions of a complex model is still of meaning.

Up to now, various analytic solutions [20,24] have been proposed by neglecting certain terms in different flow regimes. In addition, a double Dirichlet series  $h = \sum_{m=0}^{\infty} \sum_{n=0}^{\infty} a_{m,n} \exp[(mr_1 + nr_2)t]$  was used by Brittin [11] and by Xiao et al. [14], respectively, to solve the problem of capillary flows rising up monotonically to the equilibrium height. However, series solutions for the case of capillary flows fluctuating around the equilibrium height have never been presented in previous literature, to the best knowledge of authors.

In this paper, the HAM is employed to study the dynamics of capillary flows in a vertical circular tube. Unlike perturbation methods, the HAM is independent of small/large physical parameters. Also, in the framework of the HAM, we have great freedom to choose the solution expression, the auxiliary function, the auxiliary linear operator and a so-called convergence control parameter  $c_0$  which has no any physical meaning [34–40]. In the past, something new has been gained by the HAM: (1) the steady-state resonant waves were first predicted by the HAM in theory [41,42] and then confirmed experimentally [43]; (2) the solution of the steady-state resonant acoustic-gravity waves was found for the first time by means of the HAM [44]; (3) accurate results of the Stokes wave with maximum height in extremely shallow water were obtained by the HAM for the first time [45].

Utilizing the HAM, convergent series solutions of the dynamics of capillary flows are successfully obtained. In the case of capillary flows oscillating around the equilibrium height, the obtained series solution of the penetration distance of the meniscus has the basis  $\exp(m\Re[\eta_1]\tau) \cos(n\Im[\eta_1]\tau)$  and  $\exp(m\Re[\eta_1]\tau) \sin(n\Im[\eta_1]\tau)$ ; but in the case of the capillary flow rising monotonically, the series solution of the penetration distance of the meniscus can have either basis  $\exp(m\eta_1\tau)$  or basis  $\exp[(m\eta_1 + n\eta_2)\tau]$  if  $\eta_2/\eta_1 \neq \mathbb{Z}$ . Besides, it is found that the velocity of the capillary flow given by the model [15] with assumptions of constant contact angle and negligible air is larger than that of the experimental results. It is worth mentioning that the contact angle depends on both the speed and the direction of movement of the contact line [46]. The variation of the contact angle implies a friction force. Also, expelling air out of capillary also results in additional dissipation of energy; this effect is found to be significant especially for low viscous liquid [6]. So the discrepancy between our solution and experimental results should be caused by the neglect of the two damping mechanisms, the dynamic contact angle and the capillary length effect.

This paper is organized as follows. Following an introduction, the asymptotic property of the dynamics of capillary flows is given in Section 2. Procedures of the HAM for the case of capillary flows rising monotonically to the equilibrium height are presented in Section 3. Procedures of the HAM for the case of capillary flow oscillating around the equilibrium height are given in Section 4. Results and discussions are given in Section 5. Concluding remarks are given in Section 6.

## 2. Asymptotic property

Introducing two scaling factors  $H = 2\sigma \cos \theta / (\rho g r)$  and  $T = \sqrt{H/g}$  and non-dimensionalizing the penetration distance of the meniscus  $z$  and the time  $t$  by  $z = h/H$ ,  $\tau = t/T$ . Besides, defining the Bond number as  $\Omega_1 = 7\rho g r^2 / (12\sigma \cos \theta)$  and the ratio of Ohnesorge number to Bond number as  $\Omega_2 = 8\sqrt{2}\mu^2\sigma \cos \theta / (\rho^3 g^2 r^5)$ , then the Eq. (10) reduces to

$$\begin{aligned} \mathcal{N}[z(\tau)] &= \Omega \frac{d^2 z}{d\tau^2} + z - 1 + z \frac{d^2 z}{d\tau^2} + \varpi \left(\frac{dz}{d\tau}\right)^2 + \Omega_2 z \frac{dz}{d\tau} \\ &= 0 \end{aligned} \tag{12}$$

subject to boundary conditions

$$z(0) = z'(0) = 0 \tag{13}$$

with definition

$$\Omega = \begin{cases} \Omega_1 & \text{when } \frac{dz}{d\tau} \geq 0, \\ 0 & \text{when } \frac{dz}{d\tau} < 0. \end{cases} \tag{14}$$

Introducing  $z(\tau) = 1 + \varepsilon f(\tau)$  and substituting it into Eq. (12), then comparing the coefficient of  $\varepsilon$  on both sides of the equation, we gain  $(\Omega + 1)d^2 f(\tau)/d\tau^2 + \Omega_2 df(\tau)/d\tau + f(\tau) = 0$ , whose general solution is a linear combination of  $\exp[\eta_1 \tau]$  and  $\exp[\eta_2 \tau]$  with  $\eta_1 = (-\Omega_2 + \sqrt{\Omega_2^2 - 4\Omega - 4})/2(\Omega + 1)$  and  $\eta_2 = (-\Omega_2 - \sqrt{\Omega_2^2 - 4\Omega - 4})/2(\Omega + 1)$ . If  $\Omega_2 \geq 2\sqrt{\Omega_1 + 1}$ ,  $\eta_1$  and  $\eta_2$  are real for both rising and falling processes, hence the meniscus rises monotonically to the equilibrium height. If  $2\sqrt{\Omega_1 + 1} > \Omega_2 \geq 2$ ,  $\eta_1$  and  $\eta_2$  are real in the falling process but contain a non-zero imaginary part in the rising process; thus, the meniscus overshoots over the equilibrium height and then reduces to the equilibrium height. If  $\Omega_2 < 2$ , the meniscus oscillates around the equilibrium height because  $\eta_1$  and  $\eta_2$  contain non-zero imaginary parts in both rising and falling processes.

Introducing  $u = \exp[\eta_1 \tau]$  and  $w(u) = 1 - z(\tau)$ , Eqs. (12) and (13) become

$$\begin{aligned} \mathcal{N}_1[w(u)] &= (\Omega + 1)\eta_1^2 \left( u \frac{dw}{du} + u^2 \frac{d^2 w}{du^2} \right) \\ &+ w - (\Omega_2 \eta_1 + \eta_1^2) u w \frac{dw}{du} \\ &+ \Omega_2 \eta_1 u \frac{dw}{du} - \eta_1^2 u^2 w \frac{d^2 w}{du^2} \\ &- \varpi \eta_1^2 \left( u \frac{dw}{du} \right)^2 = 0 \end{aligned} \tag{15}$$

subject to boundary conditions

$$w(u) \Big|_{u=1} = 1, \quad \frac{dw(u)}{du} \Big|_{u=1} = 0, \tag{16}$$

where  $\mathcal{N}_1$  is a nonlinear operator.

## 3. The HAM approach for the meniscus motion with a monotonic path

Here we present a HAM approach for the case of meniscus rising monotonically to the equilibrium height, i.e.,  $\Omega_2 \geq 2\sqrt{\Omega_1 + 1}$ . Let  $\gamma_0(u)$  denote the initial guess of  $w(u)$ ,  $\mathcal{L}$  an auxiliary linear operator with the property  $\mathcal{L}[0] = 0$ ,  $\hat{H}(u)$  a non-zero auxiliary function,  $c_0$  a non-zero constant, called the convergence-control parameter, and  $q \in [0, 1]$  the embedding quantity, respectively. We construct following a family of differential equations

$$(1 - q)\mathcal{L}[\Gamma(u; q) - \gamma_0(u)] = c_0 q \tilde{H}(u) \mathcal{N}_1[\Gamma(u; q)], \quad (17)$$

subject to boundary conditions

$$\Gamma(u; q)\Big|_{u=1} = 1, \quad \frac{\partial \Gamma(u; q)}{\partial u}\Big|_{u=1} = 0, \quad (18)$$

where the nonlinear operator  $\mathcal{N}_1$  is defined by (15), the  $\Gamma(u; q)$  corresponds to the unknown function  $w(u)$ .

When  $q = 0$ , due to the property  $\mathcal{L}[0] = 0$ , Eq. (17) reduces to

$$\Gamma(u; 0) = \gamma_0(u). \quad (19)$$

When  $q = 1$ , Eq. (17) is equivalent to original equation (15), provided

$$\Gamma(u; 1) = w(u). \quad (20)$$

Therefore, when the embedding quantity  $q$  varies continuously from 0 to 1,  $\Gamma(u; q)$  deforms from a given initial guess  $\gamma_0(u)$  to the unknown function  $w(u)$ .

According to Eq. (19),  $\Gamma(u; q)$  can be expanded into following Maclaurin series

$$\Gamma(u; q) = \sum_{m=0}^{+\infty} \gamma_m(u) q^m, \quad (21)$$

where

$$\gamma_m(u) = \mathcal{D}_m[\Gamma(u; q)], \quad (22)$$

in which

$$\mathcal{D}_m[f] = \frac{1}{m!} \frac{\partial^m f}{\partial q^m} \Big|_{q=0} \quad (23)$$

is called the  $m$ th-order homotopy-derivative of  $f$ . Assuming that the auxiliary linear operator  $\mathcal{L}$ , the auxiliary function  $\tilde{H}(u)$  and the convergence-control parameter  $c_0$  are so properly selected that the Maclaurin series (21) is convergent at  $q = 1$ , then according to (20), we have the so-called homotopy-series solution

$$w(u) = \sum_{m=0}^{+\infty} \gamma_m(u). \quad (24)$$

Substituting (21) into the Eqs. (17), and then equating the coefficients of  $q^m$  ( $m \geq 1$ ), we have the  $m$ th-order deformation equations

$$\mathcal{L}[\gamma_m(u) - \chi_m \gamma_{m-1}(u)] = c_0 \tilde{H}(u) \delta_{m-1}(u), \quad (25)$$

subject to boundary conditions

$$\gamma_m(u)\Big|_{u=1} = 0, \quad \frac{d\gamma_m(u)}{du}\Big|_{u=1} = 0, \quad (26)$$

in which

$$\chi_m = \begin{cases} 0 & \text{when } m \leq 1, \\ 1 & \text{when } m > 1 \end{cases} \quad (27)$$

and

$$\begin{aligned} \delta_m(u) &= \mathcal{D}_m\{\mathcal{N}_1[\Gamma(u; q)]\} \\ &= (\Omega + 1)\eta_1^2 \left( u \frac{d\gamma_m}{du} + u^2 \frac{d^2\gamma_m}{du^2} \right) + \gamma_m + \Omega_2 \eta_1 u \frac{d\gamma_m}{du} \\ &\quad - \sum_{i=0}^m \left[ (\Omega_2 \eta_1 + \eta_1^2) u \gamma_i \frac{d\gamma_{m-i}}{du} + \eta_1^2 u^2 \gamma_i \frac{d^2\gamma_{m-i}}{du^2} \right. \\ &\quad \left. + \varpi \eta_1^2 u^2 \frac{d\gamma_i}{du} \frac{d\gamma_{m-i}}{du} \right]. \end{aligned} \quad (28)$$

We choose

$$\gamma_0(u) = 2u - u^2 \quad (29)$$

as the initial guess of  $w(u)$ , which satisfies the boundary conditions (18). Besides, we choose the auxiliary linear operator

$$\mathcal{L}[f] = u^2 \frac{d^2 f}{du^2} - 2u \frac{df}{du} + 2f \quad (30)$$

with the property  $\mathcal{L}[u] = \mathcal{L}[u^2] = 0$ . The corresponding inverse linear operator reads

$$\mathcal{L}^{-1}[u^m] = \frac{u^m}{(m-1)(m-2)}. \quad (31)$$

It is found that the coefficient of  $u$  in  $\delta_m(u)$  is zero, i.e.,  $\delta_m(u)$  consists of  $u^m$ ,  $m = 2, 3, 4, \dots$ . So we choose following auxiliary function

$$\tilde{H}(u) = u. \quad (32)$$

With the initial guess (29), the inverse linear operator (31) and the auxiliary function (32), the solution  $\gamma_m(u)$  of the high-order deformation equations (25) and (26) can be obtained step by step, starting from  $m = 1$ , say,

$$\begin{aligned} \gamma_m(u) &= \chi_m \gamma_{m-1}(u) + c_0 \mathcal{L}^{-1}[\tilde{H}(u) \delta_{m-1}(u)] \\ &\quad + \Lambda_1^{(m)} u + \Lambda_2^{(m)} u^2, \end{aligned} \quad (33)$$

in which  $\Lambda_1^{(m)}$  and  $\Lambda_2^{(m)}$  are constant coefficients which are determined by the boundary conditions (26).  $\gamma_m(u)$  can be expressed by

$$\gamma_m(u) = \sum_{i=1}^{3m+2} a_i^{(m)} u^i, \quad (34)$$

with the recursion formulas of  $a_i^{(m)}$ :

$$\begin{cases} a_1^{(0)} = 2, & a_2^{(0)} = -1, \\ a_i^{(m+1)} = g_i^{(m+1)} + \chi_{3-i} \Lambda_1^{(m+1)} + (\chi_{4-i} - \chi_{3-i}) \Lambda_2^{(m+1)}, \end{cases} \quad (35)$$

where

$$g_i^{(m+1)} = \begin{cases} \chi_{m+1} a_i^{(m)}, & i = 1, 2 \\ \chi_{m+1} \chi_{3m+4-i} a_i^{(m)} \\ \quad + \frac{c_0 [\Delta_{i-1}^{(1,m+1)} - \Delta_{i-1}^{(2,m+1)}]}{(i-1)(i-2)}, & i > 2, \end{cases} \quad (36)$$

$$\begin{aligned} \Delta_i^{(1,m+1)} &= \chi_{3m+4-i} \left\{ (\Omega + 1) \eta_1^2 [b_i^{(m)} + c_i^{(m)}] \right. \\ &\quad \left. + a_i^{(m)} + \Omega_2 \eta_1 b_i^{(m)} \right\}, \end{aligned} \quad (37)$$

$$\begin{aligned} \Delta_i^{(2,m+1)} &= \sum_{n=0}^m \left[ (\Omega_2 \eta_1 + \eta_1^2) d_i^{(n,m+1)} + \eta_1^2 e_i^{(n,m+1)} \right. \\ &\quad \left. + \varpi \eta_1^2 f_i^{(n,m+1)} \right], \end{aligned} \quad (38)$$

$$\Lambda_1^{(m+1)} = \sum_{i=1}^{3m+5} (i-2) g_i^{(m+1)}, \quad \Lambda_2^{(m+1)} = \sum_{i=1}^{3m+5} (1-i) g_i^{(m+1)}, \quad (39)$$

in which

$$b_i^{(n)} = i a_i^{(n)}, \quad c_i^{(n)} = (i-1) b_i^{(n)}, \quad (40)$$

<sup>2</sup> Detailed derivation is given in Appendix A.

$$d_i^{(n,m+1)} = \sum_{j=\max\{1,i+3n-3m-2\}}^{\min\{3n+2,i-1\}} a_j^{(n)} b_{i-j}^{(m-n)}, \quad (41)$$

$$e_i^{(n,m+1)} = \sum_{j=\max\{1,i+3n-3m-2\}}^{\min\{3n+2,i-1\}} a_j^{(n)} c_{i-j}^{(m-n)}, \quad (42)$$

$$f_i^{(n,m+1)} = \sum_{j=\max\{1,i+3n-3m-2\}}^{\min\{3n+2,i-1\}} b_j^{(n)} b_{i-j}^{(m-n)}. \quad (43)$$

The  $M$ th-order homotopy-approximation of  $w(u)$  reads

$$\tilde{w}_M(u) = \sum_{m=0}^M \gamma_m(u). \quad (44)$$

#### 4. The HAM approach for the meniscus motion with an oscillatory path

In this section, we propose another HAM approach for the case of meniscus oscillating around the equilibrium height, i.e.,  $\Omega_2 < 2\sqrt{\Omega_1 + 1}$ . Let us consider the model (12) subjecting to following boundary conditions

$$z(\tau_0) = \zeta, \quad z'(\tau_0) = 0. \quad (45)$$

With transformation  $u = \exp[\eta_1 \tau]$  and  $w(u) = 1 - z(\tau)$ , the governing equation (12) becomes (15) and the boundary conditions (45) become

$$w(u) \Big|_{u=\exp[\eta_1 \tau_0]} = 1 - \zeta, \quad \frac{dw(u)}{du} \Big|_{u=\exp[\eta_1 \tau_0]} = 0. \quad (46)$$

Similar to Section 3, we construct a family of equations

$$(1 - q)\mathcal{L}[\Gamma(u; q) - \gamma_0(u)] = c_0 q \mathcal{N}_1[\Gamma(u; q)] \quad (47)$$

subject to boundary conditions

$$\Gamma(u; q) \Big|_{u=e^{\eta_1 \tau_0}} = 1 - \zeta, \quad \frac{\partial \Gamma(u; q)}{\partial u} \Big|_{u=e^{\eta_1 \tau_0}} = 0, \quad (48)$$

where the nonlinear operator  $\mathcal{N}_1$  is defined by (15).

When  $q = 0$ , Eq. (47) reduces to

$$\Gamma(u; 0) = \gamma_0(u). \quad (49)$$

When  $q = 1$ , Eq. (47) is equivalent to original equation (15), provided

$$\Gamma(u; 1) = w(u). \quad (50)$$

So  $\Gamma(u; q)$  deforms from initial guess  $\gamma_0(u)$  to the unknown function  $w(u)$  as  $q$  varies continuously from 0 to 1. Again, we expand  $\Gamma(u; q)$  into Maclaurin series

$$\Gamma(u; q) = \sum_{m=0}^{+\infty} \gamma_m(u) q^m. \quad (51)$$

If above Maclaurin series is convergent at  $q = 1$ , then the homotopy-series solution reads

$$w(u) = \sum_{m=0}^{+\infty} \gamma_m(u). \quad (52)$$

Substituting Eq. (51) into Eqs. (47) and (48), we have the  $m$ th-order deformation equations

$$\mathcal{L}[\gamma_m(u) - \chi_m \gamma_{m-1}(u)] = c_0 \delta_{m-1}(u), \quad (53)$$

subject to boundary conditions

$$\gamma_m(u) \Big|_{u=e^{\eta_1 \tau_0}} = 0, \quad \frac{d\gamma_m(u)}{du} \Big|_{u=e^{\eta_1 \tau_0}} = 0, \quad (54)$$

in which  $\chi_m$  and  $\delta_m(u)$  are defined by (27) and (28), respectively.

Motivated by the two time scales  $\eta_1$  and  $\eta_2$  obtained in Section 2, we choose

$$\gamma_0(u) = \frac{1 - \zeta}{\eta_1 - \eta_2} \left[ \frac{\eta_1}{e^{\eta_2 \tau_0}} u^{\eta_2/\eta_1} - \frac{\eta_2 u}{e^{\eta_1 \tau_0}} \right] \quad (55)$$

as the initial guess of  $w(u)$ , which satisfies the boundary conditions (46). It is found that both the coefficients of  $u$  and  $u^{\eta_2/\eta_1}$  in  $\delta_m(u)$  are zero, i.e.,  $\delta_m(u)$  consists of  $u^{m+n\eta_2/\eta_1}$ ,  $m+n = 2, 3, 4, \dots$ . So we choose the auxiliary linear operator

$$\mathcal{L}[f] = \eta_1^2 u^2 \frac{d^2 f}{du^2} - \eta_1 \eta_2 u \frac{df}{du} + \eta_1 \eta_2 f \quad (56)$$

with the property  $\mathcal{L}[u] = \mathcal{L}[u^{\eta_2/\eta_1}] = 0$ . The corresponding inverse linear operator reads

$$\mathcal{L}^{-1}[u^m] = \frac{u^m}{\eta_1(m-1)(m\eta_1 - \eta_2)}. \quad (57)$$

Using the initial guess (55) and the inverse linear operator (57), the solution  $\gamma_m(u)$  of the high-order deformation equations (53) and (54) can be obtained step by step, starting from  $m = 1$ , say,

$$\gamma_m(u) = \chi_m \gamma_{m-1}(u) + c_0 \mathcal{L}^{-1}[\delta_{m-1}(u)] + \Lambda_3^{(m)} u + \Lambda_4^{(m)} u^{\eta_2/\eta_1}, \quad (58)$$

in which  $\Lambda_3^{(m)}$  and  $\Lambda_4^{(m)}$  are constant coefficients which are determined by the boundary conditions (54).  $\gamma_m(u)$  can be expressed by

$$\gamma_m(u) = \sum_{i=0}^{m+1} \sum_{j=\max\{1-i,0\}}^{m+1-i} a_{i,j}^{(m)} u^{i+j\eta_2/\eta_1} \quad (59)$$

with the recursion formula of  $a_{i,j}^{(m)}$ :

$$\begin{cases} a_{0,1}^{(0)} = \frac{(1-\zeta)\eta_1}{(\eta_1 - \eta_2)e^{\eta_2 \tau_0}}, & a_{1,0}^{(0)} = \frac{(1-\zeta)\eta_2}{(\eta_2 - \eta_1)e^{\eta_1 \tau_0}}, \\ a_{i,j}^{(m+1)} = g_{i,j}^{(m+1)} + (1 - \chi_i)(1 - \chi_{j+1})\Lambda_1^{(m+1)} \\ \quad + (1 - \chi_{i+1})(1 - \chi_j)\Lambda_2^{(m+1)}, \end{cases} \quad (60)$$

where

$$g_{i,j}^{(m+1)} = \begin{cases} \chi_{m+1} a_{i,j}^{(m)}, & i+j = 1, \\ \chi_{m+1} \chi_{m+3-i-j} a_{i,j}^{(m)} \\ \quad + \frac{c_0 [\Delta_{i,j}^{(1,m+1)} - \Delta_{i,j}^{(2,m+1)}]}{[(i-1)\eta_1 + j\eta_2][i\eta_1 + (j-1)\eta_2]}, & i+j > 1, \end{cases} \quad (61)$$

$$\Delta_{i,j}^{(1,m+1)} = \chi_{m+3-i-j} \left\{ (\Omega_2 + 1)\eta_1^2 [b_{i,j}^{(m)} + c_{i,j}^{(m)}] + a_{i,j}^{(m)} + \Omega_2 \eta_1 b_{i,j}^{(m)} \right\}, \quad (62)$$

$$\Delta_{i,j}^{(2,m+1)} = \sum_{n=0}^m [(\Omega_2 \eta_1 + \eta_1^2) d_{i,j}^{(n,m+1)} + \eta_1^2 e_{i,j}^{(n,m+1)} + \varpi \eta_1^2 f_{i,j}^{(n,m+1)}], \quad (63)$$

$$\Lambda_3^{(m+1)} = \sum_{i=0}^{m+2} \sum_{j=\max\{1-i,0\}}^{m+2-i} \frac{g_{i,j}^{(m+1)}}{\eta_2 - \eta_1} [i\eta_1 + (j-1)\eta_2], \quad (64)$$

<sup>3</sup> Detailed derivation is given in Appendix B.

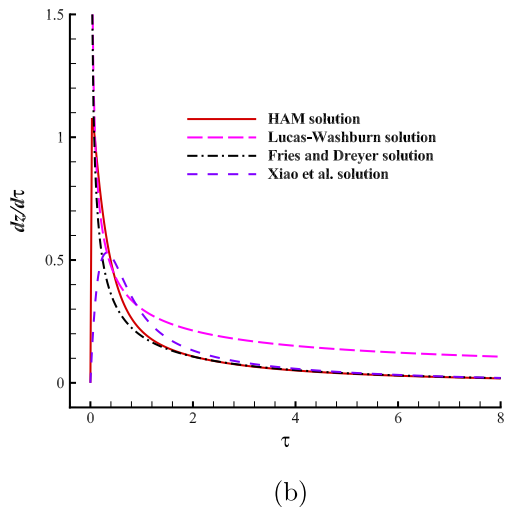
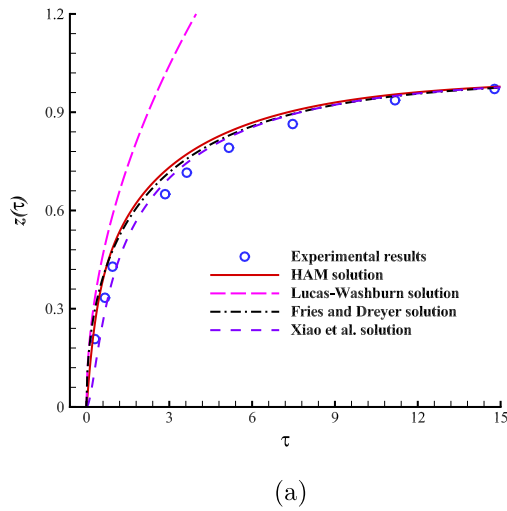


**Fig. 2.** Dimensionless penetration distance  $z$  and the velocity  $dz/d\tau$  of the meniscus versus dimensionless time  $\tau$ .  $\rho = 1000 \text{ kg/m}^3$ ,  $\mu = 0.001 \text{ Pa s}$ ,  $\sigma = 0.072 \text{ N/m}$ ,  $g = 9.81 \text{ m/s}^2$ , contact angle  $\theta = 0$ , radius of capillary tube  $r = 0.0316 \text{ cm}$ .  $\circ$ , experimental results [47]; —, homotopy-series solution of the model (12); - - -, analytic solutions  $z = 1 + W[-\exp(-1 - \tau/\Omega_2)]$ , in which  $W$  is Lambert  $W$  function with property  $x = W(x)\exp[W(x)]$ , given by Fries and Dreyer [20]; - · -, analytic solutions given by Xiao et al. [14].

$$A_4^{(m+1)} = \sum_{i=0}^{m+2} \sum_{j=\max\{1-i,0\}}^{m+2-i} \frac{g_{i,j}^{(m+1)}}{\eta_2 - \eta_1} \left[ (1-i)\eta_1 - j\eta_2 \right], \quad (65)$$

in which

$$b_{i,j}^{(n)} = a_{i,j}^{(n)} \left( i + j \frac{\eta_2}{\eta_1} \right), \quad c_{i,j}^{(n)} = b_{i,j}^{(n)} \left( i - 1 + j \frac{\eta_2}{\eta_1} \right), \quad (66)$$

$$d_{i,j}^{(n,m+1)} = \sum_{p=\max\{0,1-j,i-m+n-1\}}^{\min\{i,n+1,i+j-1\}} \sum_{r=\max\{0,1-p,i+j-m+n-1-p\}}^{\min\{j,n+1-p,i+j-1-p\}} a_{p,r}^{(n)} \times b_{i-p,j-r}^{(m-n)} \quad (67)$$

$$e_{i,j}^{(n,m+1)} = \sum_{p=\max\{0,1-j,i-m+n-1\}}^{\min\{i,n+1,i+j-1\}} \sum_{r=\max\{0,1-p,i+j-m+n-1-p\}}^{\min\{j,n+1-p,i+j-1-p\}} a_{p,r}^{(n)} \times c_{i-p,j-r}^{(m-n)}, \quad (68)$$

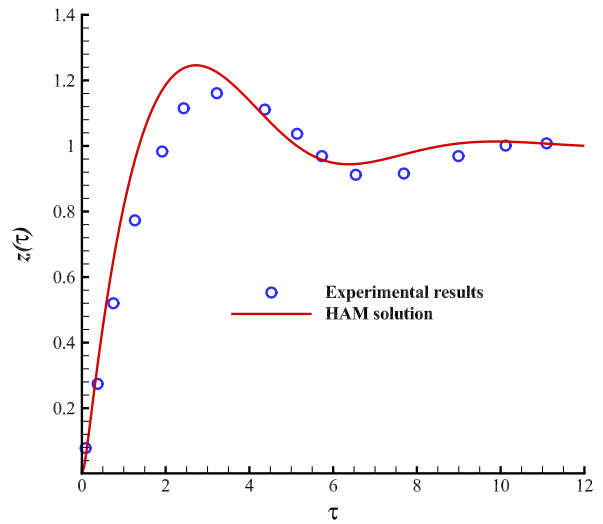


**Fig. 3.** Dimensionless penetration distance  $z$  of the meniscus versus dimensionless time  $\tau$ .  $\rho = 710 \text{ kg/m}^3$ ,  $\mu = 0.0006 \text{ Pa s}$ ,  $\sigma = 0.0167 \text{ N/m}$ ,  $g = 9.81 \text{ m/s}^2$ , contact angle  $\theta = 0$ , radius of capillary tube  $r = 0.5 \text{ mm}$ .  $\circ$ , experimental results [6]; —, homotopy-series solution of the model (12);

$$f_{i,j}^{(n,m+1)} = \sum_{p=\max\{0,1-j,i-m+n-1\}}^{\min\{i,n+1,i+j-1\}} \sum_{r=\max\{0,1-p,i+j-m+n-1-p\}}^{\min\{j,n+1-p,i+j-1-p\}} b_{p,r}^{(n)} b_{i-p,j-r}^{(m-n)}. \quad (69)$$

The  $M$ th-order homotopy-approximation of  $w(u)$  reads

$$\tilde{w}_M(u) = \sum_{m=0}^M \gamma_m(u). \quad (70)$$

### 5. Results and discussions

We firstly validate the HAM approaches proposed in Sections 3 and 4. It is worth mentioning that we are free to select an appropriate convergence control parameter  $c_0$ , which has no physical meaning, to obtain a convergent homotopy-series solution. According to our computation, approaching a negative  $c_0$  to zero can effectively yield a convergent homotopy-series solution but reduce the convergence rate. Series solutions are convergent when using  $-(60\Omega_2 + 3)/[(5\Omega + 5)(10\Omega_2 + 1)] \leq c_0 < 0$  for both the HAM approaches proposed in Sections 3 and 4. However, from the viewpoint of efficiency,  $c_0 = -(60\Omega_2 + 3)/[(5\Omega + 5)(10\Omega_2 + 1)]$  is suggested.

The comparisons of the homotopy-series solution of the model (12) and several other analytic solutions [9,10,14] against the experimental results are as shown in Fig. 2(a). The penetration distance of the meniscus given by the model (12) is larger than the experimental results. This discrepancy should be caused by the two assumptions used in the paper: both the variation of the contact angle  $\theta$  and the gas effect are assumed to be negligible. In practice, the contact angle depends on the speed and direction of movement of the contact line [46]. The contact angle is found to reduce to virtually zero as the liquid rises to the equilibrium position [46], so simplifying the dynamic contact angle to a constant value  $\theta = 0$  exaggerates the surface tension effect and hence overestimates the velocity of the meniscus, as shown in Fig. 2 (a). Besides, the additional viscous drag due to

<sup>4</sup> Numerous combinations for  $0.0001 \leq \Omega_1, \Omega_2 \leq 100$  are examined.

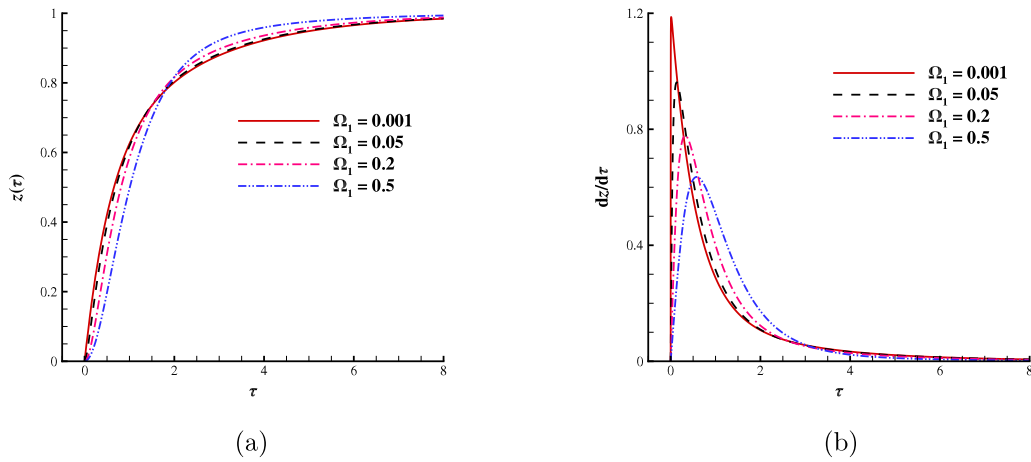


Fig. 4. Homotopy-series solutions of the penetration distance  $z$  and the velocity  $dz/d\tau$  in the case of  $\Omega_2 = 3$ .

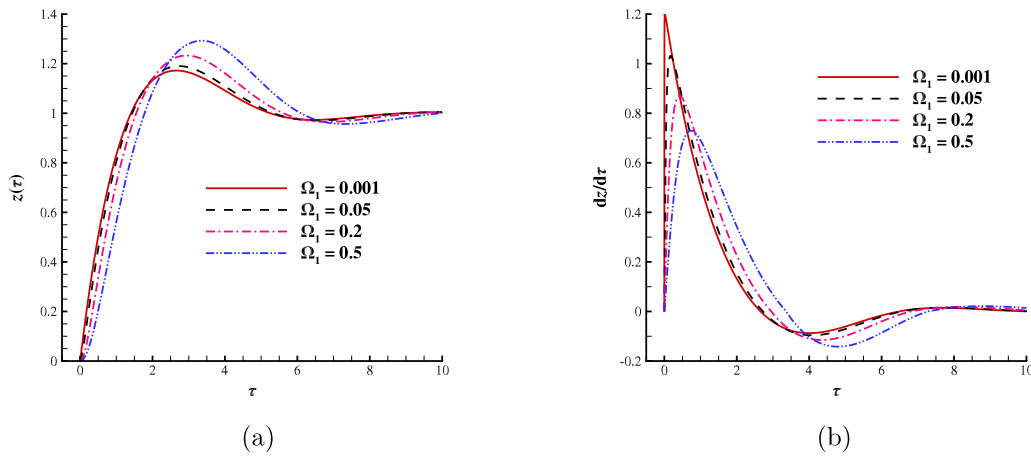


Fig. 5. Homotopy-series solutions of the penetration distance  $z$  and the velocity  $dz/d\tau$  in the case of  $\Omega_2 = 1$ .

the air being expelled from capillary by rising liquid is found to be significant for low viscous liquid [6]. As shown in Fig. 2(a) and (b), the analytic solution  $z = 1 + W[-\exp(-1 - \tau/\Omega_2)]$ , in which  $W$  is Lambert  $W$  function with property  $x = W(x)\exp[W(x)]$ , gives similar results of the penetration distance of the meniscus as our homotopy-series solution, although the velocity given by the solution  $z = 1 + W[-\exp(-1 - \tau/\Omega_2)]$  is infinite as  $\tau \rightarrow 0$ . Fig. 3 compares the homotopy-series solution of the model (12) and the experimental results. Again, the damping rate described by the model (12) is less than the practical situation.

It is worth mentioning that the inertial effect dominates the capillary flow at the initial stage. Therefore, enlarging  $\Omega_1$ , which is the Bond number that denotes the ratio of gravitational forces to surface tension forces, while fixing  $\Omega_2$ , which is the ratio of Ohnesorge number to Bond number, should reduce the acceleration of the capillary flow at the initial stage. By contrast, fixing  $\Omega_1$  but enlarging  $\Omega_2$  should have little effect on the velocity of the meniscus at the initial stage. These are demonstrated by Figs. 4–6. In addition, as shown in Fig. 6, the amplitude decreases quickly with enlarging  $\Omega_2$ , which illustrates that the viscous force indeed becomes significant in the latter stage.

Here it should be mentioned that in the case of capillary flows rising monotonically,  $\Im[\eta_1] = \Im[\eta_2] = 0$ , both the series solution with the basis  $\exp[m\eta_1\tau]$ ,  $m \in \mathbb{Z}^+$ , proposed in Section 3, and the series solution with the basis  $\exp[(m\eta_1 + n\eta_2)\tau]$ , proposed in

Section 4 are valid. In the case of capillary flows oscillating around equilibrium height,  $\Im[\eta_1] = -\Im[\eta_2] \neq 0$ , the series solution proposed in Section 4 has the basis  $\exp(m\Re[\eta_1]\tau)\cos(n\Im[\eta_1]\tau)$  and  $\exp(m\Re[\eta_1]\tau)\sin(n\Im[\eta_1]\tau)$ . The explicit series solution of the oscillatory case, to the best knowledge of authors, is never presented previously. At last, it is worth mentioning that there is only the viscosity term,  $\Omega_2 z \, dz/d\tau$ , in the model (12) that damps the energy out. If a inviscid liquid, i.e.,  $\Omega_2 = 0$ , is considered, the amplitude of the penetration distance of the meniscus will remain unchanged as time, which is characterized by our series solution that has basis  $\cos(n\Im[\eta_1]\tau)$  and  $\sin(n\Im[\eta_1]\tau)$ ,  $n \in \mathbb{Z}$ . But if both the dynamic contact angle and the expulsion of the air out of the capillary are taken into account, the energy should be gradually damped out, which is the practical case.

### 6. Concluding remarks

In this paper, the homotopy analysis method is applied to study the dynamics of capillary flows in a vertical circular tube. The model (10), proposed by Maggi and Alonso-Marroquin [15], is considered but based on the assumptions of the constant contact angle and of the negligible gas. Two dimensionless parameters  $\Omega_1 = 7\rho g r^2 / (12\sigma \cos\theta)$ , the Bond number, and  $\Omega_2 = 8\sqrt{2\mu^2\sigma \cos\theta} / (\rho^3 g^2 r^5)$ , the ratio of Ohnesorge number to Bond number, are studied. When  $\Omega_2 < 2$ , the meniscus fluctuates

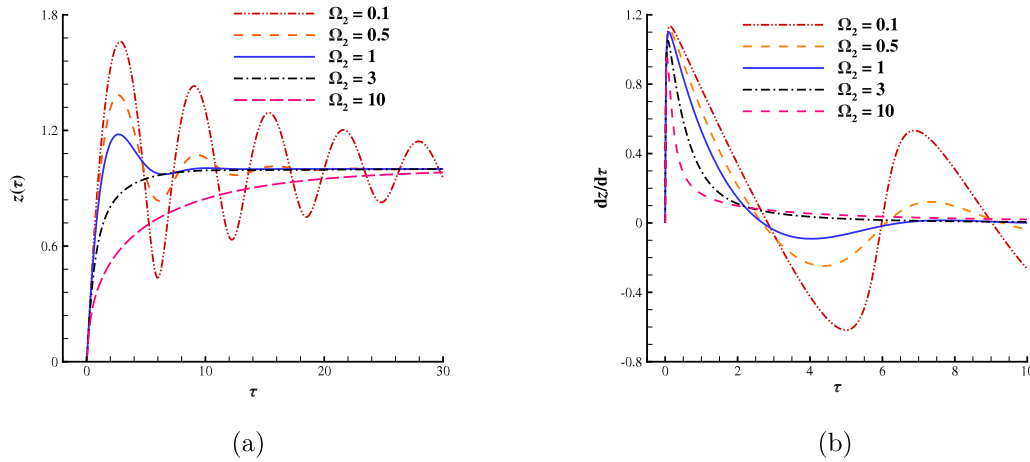


Fig. 6. Homotopy-series solutions of the penetration distance  $z$  in the case of  $\Omega_1 = 0.02$ .

around the equilibrium height; when  $2\sqrt{\Omega_1 + 1} > \Omega_2 \geq 2$ , the capillary flow overshoots over the equilibrium height and then reduces to the equilibrium height. Both these two oscillating behavior can be described by the homotopy-series solution with basis  $\exp(m\Im[\eta_1]\tau) \cos(n\Re[\eta_1]\tau)$  and  $\exp(m\Im[\eta_1]\tau) \sin(n\Re[\eta_1]\tau)$ ,  $\eta_1 = (-\Omega_2 + \sqrt{\Omega_2^2 - 4\Omega - 4})/2(\Omega + 1)$ ,  $m \in \mathbb{Z}^+$ ,  $n \in \mathbb{Z}$ . When  $\Omega_2 \geq 2\sqrt{\Omega_1 + 1}$ , the capillary flow rises monotonically to the equilibrium position. This behavior can be characterized by either the homotopy-series solution with basis  $\exp[m\eta_1\tau]$ ,  $m \in \mathbb{Z}^+$ , or the homotopy-series solution with basis  $\exp[(m\eta_1 + n\eta_2)\tau]$ .

The effects of the dimensionless parameters  $\Omega_1$  and  $\Omega_2$  on the dynamics of capillary flows are also studied. The velocity of the meniscus at the initial stage is only dependent on the  $\Omega_1$ , but the  $\Omega_2$  has significant effects on determining the damping rate of amplitude, as shown in Figs. 4–6. So the capillary flow is dominated by the inertial effect at the initial stage but the viscous effect becomes significant in the latter stage, these results are consistent with that of previous literature [16,17,19].

However, our computed penetration distance of the meniscus is larger than that of the experimental results. This discrepancy should be mainly caused by the two assumptions used in this paper: (1) the contact angle remains constant; (2) the gas is negligible. Hamraoui et al. [46] analyzed the dynamic contact angle in detail and found that the dynamic contact angle decreases to virtually zero. Besides, Hamraoui et al. [46] proposed that the significant variation of contact angle  $\theta$  implies a friction force, which can be expressed as  $F = \sigma[(\cos\theta_0 - \cos\theta)] = \beta(dz/dt)^n$ , where  $\beta$  is a molecular parameter that can be defined as a friction coefficient,  $\theta_0$  is the equilibrium contact angle. Moreover, Zhmud et al. [6] studied the capillary length effect and found that taking the air into account would result in additional dissipation of energy. The corresponding viscous drag can be expressed as  $8\pi\mu_g(L - z)dz/dt$ , in which  $\mu_g$  and  $L$  denote the gas viscosity and the capillary length, respectively. Zhmud et al. [6] also pointed out that the capillary effect can be significant for low viscous liquids. To sum up, the two assumptions used in this paper result in the neglect of two potential damping mechanisms. Therefore, a more comprehensive model including the dynamic contact angle and the capillary length effect needs to be considered.

## Acknowledgments

Thanks to anonymous reviewers for their valuable comments and suggestions. This work is partly supported by National Natural Science Foundation of China (Approval No. 11432009).

## Appendix A. The recursion formulas of $a_i^{(m)}$ in (35)

Here we derive the recursion formulas of  $a_i^{(m)}$  in (35). According to (29) and (34), it is easy to gain  $a_1^{(0)} = 2$  and  $a_2^{(0)} = -1$ . Assuming that for any  $n \leq m$ ,  $\gamma_n(u)$  can be expressed as

$$\gamma_n(u) = \sum_{i=1}^{3n+2} a_i^{(n)} u^i = \sum_{i=2}^{3n+4} \chi_{3n+4-i} a_i^{(n)} u^i + a_1^{(n)} u, \quad (\text{A.1})$$

in which  $\chi_n$  is defined by (27). Then for any  $n \leq m$ , it holds

$$\begin{cases} u \frac{d\gamma_n}{du} = \sum_{i=1}^{3n+2} b_i^{(n)} u^i = \sum_{i=2}^{3n+4} \chi_{3n+4-i} b_i^{(n)} u^i + b_1^{(n)} u, \\ u^2 \frac{d^2\gamma_n}{du^2} = \sum_{i=2}^{3n+2} c_i^{(n)} u^i = \sum_{i=2}^{3n+4} \chi_{3n+4-i} c_i^{(n)} u^i, \end{cases} \quad (\text{A.2})$$

in which  $b_i^{(n)}$  and  $c_i^{(n)}$  are defined by (40).

Using (A.1) and (A.2), it is easy to derive

$$\begin{aligned} \gamma_n \left( u \frac{d\gamma_{m-n}}{du} \right) &= \left[ \sum_{i=1}^{3n+2} a_i^{(n)} u^i \right] \left[ \sum_{i=1}^{3m-3n+2} b_i^{(m-n)} u^i \right] \\ &= \sum_{i=2}^{3m+4} d_i^{(n,m+1)} u^i, \end{aligned} \quad (\text{A.3})$$

where  $d_i^{(n,m+1)}$  is defined by (41). Similarly, we have

$$\gamma_n \left( u^2 \frac{d^2\gamma_{m-n}}{du^2} \right) = \sum_{i=2}^{3m+4} e_i^{(n,m+1)} u^i, \quad (\text{A.4})$$

$$\left( u \frac{d\gamma_n}{du} \right) \left( u \frac{d\gamma_{m-n}}{du} \right) = \sum_{i=2}^{3m+4} f_i^{(n,m+1)} u^i, \quad (\text{A.5})$$

where  $e_i^{(n,m+1)}$  and  $f_i^{(n,m+1)}$  are defined by (42) and (43) respectively. Then according to (28) and (A.1)–(A.5), we gain

$$\delta_m = \sum_{i=2}^{3m+4} \left[ \Delta_i^{(1,m+1)} - \Delta_i^{(2,m+1)} \right] u^i, \quad (\text{A.6})$$

where  $\Delta_i^{(1,m+1)}$  and  $\Delta_i^{(2,m+1)}$  are defined by (37) and (38).

Using (32), (31), (33), (A.1) and (A.6), we have

$$\begin{aligned} \gamma_{m+1} &= \chi_{m+1} \gamma_m + c_0 \mathcal{L}^{-1}[\tilde{H}(u) \delta_m] + \Lambda_1^{(m+1)} u + \Lambda_2^{(m+1)} u^2 \\ &= \left[ \sum_{i=1}^{3m+5} g_i^{(m+1)} u^i \right] + \Lambda_1^{(m+1)} u + \Lambda_2^{(m+1)} u^2, \end{aligned} \quad (\text{A.7})$$

in which  $g_i^{(m+1)}$  is defined by (36).  $\Lambda_1^{(m+1)}$  and  $\Lambda_2^{(m+1)}$  are determined by the boundary conditions (26). In addition,  $u$  and  $u^2$  can also be expressed as

$$u = \sum_{i=1}^{3m+5} \chi_{3-i} u^i, \quad u^2 = \sum_{i=1}^{3m+5} (\chi_{4-i} - \chi_{3-i}) u^i. \tag{A.8}$$

Substituting (A.8) into (A.7), we have

$$\gamma_{m+1} = \sum_{i=1}^{3m+5} a_i^{(m+1)} u^i, \tag{A.9}$$

in which  $a_i^{(m+1)}$  is defined by (35).

**Appendix B. The recursion formulas of  $a_{i,j}^{(m)}$  in (60)**

Here we derive the recursion formulas of  $a_{i,j}^{(m)}$  in (60). According to (55) and (59), it is easy to gain  $a_{0,1}^{(0)} = (1 - \zeta)\eta_1/(\eta_1 - \eta_2)e^{\eta_2\tau_0}$  and  $a_{1,0}^{(0)} = (1 - \zeta)\eta_2/(\eta_2 - \eta_1)e^{\eta_1\tau_0}$ . Assuming that for any  $n \leq m$ ,  $\gamma_n(u)$  can be expressed as

$$\begin{aligned} \gamma_n(u) &= \sum_{i=0}^{n+1} \sum_{j=\max\{1-i,0\}}^{n+1-i} a_{i,j}^{(n)} u^{i+j\eta_2/\eta_1} \\ &= \sum_{i=0}^{n+2} \sum_{j=\max\{1-i,0\}}^{n+2-i} \chi_{n+3-i-j} a_{i,j}^{(n)} u^{i+j\eta_2/\eta_1}, \end{aligned} \tag{B.1}$$

where  $\chi_n$  is defined by (27). Then for any  $n \leq m$ , it holds

$$\begin{cases} u \frac{d\gamma_n}{du} = \sum_{i=0}^{n+1} \sum_{j=\max\{1-i,0\}}^{n+1-i} b_{i,j}^{(n)} u^{i+j\eta_2/\eta_1} \\ \quad = \sum_{i=0}^{n+2} \sum_{j=\max\{1-i,0\}}^{n+2-i} \chi_{n+3-i-j} b_{i,j}^{(n)} u^{i+j\eta_2/\eta_1}, \\ u^2 \frac{d^2\gamma_n}{du^2} = \sum_{i=0}^{n+1} \sum_{j=\max\{1-i,0\}}^{n+1-i} c_{i,j}^{(n)} u^{i+j\eta_2/\eta_1} \\ \quad = \sum_{i=0}^{n+2} \sum_{j=\max\{1-i,0\}}^{n+2-i} \chi_{n+3-i-j} c_{i,j}^{(n)} u^{i+j\eta_2/\eta_1}, \end{cases} \tag{B.2}$$

in which  $b_{i,j}^{(n)}$  and  $c_{i,j}^{(n)}$  are defined by (40).

According to (B.1) and (B.2), we have

$$\begin{aligned} &\gamma_n \left( u \frac{d\gamma_{m-n}}{du} \right) \\ &= \left( \sum_{p=0}^{n+1} \sum_{r=\max\{1-p,0\}}^{n+1-p} a_{p,r}^{(n)} u^{p+r\eta_2/\eta_1} \right) \\ &\quad \times \left( \sum_{s=0}^{m-n+1} \sum_{t=\max\{1-s,0\}}^{m-n+1-s} b_{s,t}^{(m-n)} u^{s+t\eta_2/\eta_1} \right) \\ &= \sum_{i=0}^{m+2} \sum_{j=\max\{1-i,0\}}^{m+2-i} d_{i,j}^{(n,m+1)} u^{i+j\eta_2/\eta_1}, \end{aligned} \tag{B.3}$$

where  $d_{i,j}^{(n,m+1)}$  is defined by (67). Similarly, we have

$$\begin{aligned} \gamma_n \left( u^2 \frac{d^2\gamma_{m-n}}{du^2} \right) &= \sum_{i=0}^{m+2} \sum_{j=\max\{1-i,0\}}^{m+2-i} e_{i,j}^{(n,m+1)} u^{i+j\eta_2/\eta_1}, \\ \left( u \frac{d\gamma_n}{du} \right) \left( u \frac{d\gamma_{m-n}}{du} \right) &= \sum_{i=0}^{m+2} \sum_{j=\max\{1-i,0\}}^{m+2-i} f_{i,j}^{(n,m+1)} u^{i+j\eta_2/\eta_1}, \end{aligned} \tag{B.4}$$

where  $e_{i,j}^{(n,m+1)}$  and  $f_{i,j}^{(n,m+1)}$  are defined by (68) and (69), respectively. Then according to (28) and (B.1)–(B.4), we gain

$$\delta_m = \sum_{i=0}^{m+2} \sum_{j=\max\{1-i,0\}}^{m+2-i} \left[ \Delta_{i,j}^{(1,m+1)} - \Delta_{i,j}^{(2,m+1)} \right] u^{i+j\eta_2/\eta_1}, \tag{B.5}$$

where  $\Delta_{i,j}^{(1,m+1)}$  and  $\Delta_{i,j}^{(2,m+1)}$  are defined by (62) and (63).

Using (57), (58), (B.1) and (B.5), we have

$$\begin{aligned} \gamma_{m+1} &= \chi_{m+1}\gamma_m + c_0\mathcal{L}^{-1}[\delta_m] + \Lambda_1^{(m+1)}u + \Lambda_2^{(m+1)}u^{\eta_2/\eta_1} \\ &= \left( \sum_{i=0}^{m+2} \sum_{j=\max\{1-i,0\}}^{m+2-i} g_{i,j}^{(m+1)} u^i u_c^j \right) + \Lambda_1^{(m+1)}u + \Lambda_2^{(m+1)}u^{\eta_2/\eta_1}, \end{aligned} \tag{B.6}$$

in which  $g_{i,j}^{(m+1)}$  is defined by (61).  $\Lambda_3^{(m+1)}$  and  $\Lambda_4^{(m+1)}$  are determined by boundary conditions (54). In addition,  $u$  and  $u_c$  can be expressed as

$$\begin{cases} u = \sum_{i=0}^{m+2} \sum_{j=\max\{1-i,0\}}^{m+2-i} (1 - \chi_i)(1 - \chi_{j+1}) u^{i+j\eta_2/\eta_1}, \\ u^{\eta_2/\eta_1} = \sum_{i=0}^{m+2} \sum_{j=\max\{1-i,0\}}^{m+2-i} (1 - \chi_{i+1})(1 - \chi_j) u^{i+j\eta_2/\eta_1}. \end{cases} \tag{B.7}$$

Substituting (B.7) into (B.6), we have

$$\gamma_{m+1} = \sum_{i=0}^{m+2} \sum_{j=\max\{1-i,0\}}^{m+2-i} a_{i,j}^{(m+1)} u^{i+j\eta_2/\eta_1}, \tag{B.8}$$

in which  $a_{i,j}^{(m+1)}$  is defined by (60).

**References**

- [1] C.H. Bosanquet, On the flow of liquids into capillary tubes, London Edinburgh Dublin Phil. Mag. J. Sci. 45 (1923) 525–531, <http://dx.doi.org/10.1080/14786442308634144>.
- [2] L.R. Fisher, P.D. Lark, An experimental study of the Washburn equation for liquid flow in very fine capillaries, J. Colloid Interface Sci. 69 (1979) 486–492.
- [3] A.A. Jeje, Rates of spontaneous movement of water in capillary tubes, J. Colloid Interface Sci. 69 (1979) 420–429.
- [4] P. Joos, P. Van Remoortere, M. Bracke, The kinetics of wetting in a capillary, J. Colloid Interface Sci. 136 (1990) 189–197.
- [5] N. Ichikawa, Y. Satoda, Interface dynamics of capillary flow in a tube under negligible gravity condition, J. Colloid Interface Sci. 162 (1994) 350–355.
- [6] B.V. Zhmud, F. Tiberg, K. Hallstenson, Dynamics of capillary rise, J. Colloid Interface Sci. 228 (2000) 263–269.
- [7] N. Fries, M. Dreyer, Dimensionless scaling methods for capillary rise, J. Colloid Interface Sci. 338 (2009) 514–518, <http://dx.doi.org/10.1016/j.jcis.2009.06.036>.
- [8] J.M. Bell, F.K. Cameron, The flow of liquids through capillary spaces, J. Phys. Chem. 10 (1906) 658–674.
- [9] R. Lucas, Ueber das Zeitgesetz des kapillaren Aufstiegs von Flüssigkeiten, Kolloid-Z. 23 (1918) 15–22, <http://dx.doi.org/10.1007/BF01461107>.
- [10] E.W. Washburn, The dynamics of capillary flow, Phys. Rev. 17 (1921) 273–283, <http://dx.doi.org/10.1103/PhysRev.17.273>.
- [11] V.E. Brittin, Liquid rise in a capillary tube, J. Appl. Phys. 17 (1946) 37–44.
- [12] J. Szekeley, A. Neumann, Y. Chuang, The rate of capillary penetration and the applicability of the washburn equation, J. Colloid Interface Sci. 35 (1971) 273–278, [http://dx.doi.org/10.1016/0021-9797\(71\)90120-2](http://dx.doi.org/10.1016/0021-9797(71)90120-2).
- [13] S. Levine, P. Reed, E.J. Watson, G. Neale, A theory of the rate of rise of a liquid in a capillary, Colloid Interface Sci. (1976) 403–419.
- [14] Y. Xiao, F.Z. Yang, R. Pitchumani, A generalized analysis of capillary flows in channels, J. Colloid Interface Sci. 298 (2006) 880–888, <http://dx.doi.org/10.1016/j.jcis.2006.01.005>.
- [15] F. Maggi, F. Alonzo-Marroquin, Multiphase capillary flows, Int. J. Multiph. Flow. 42 (2012) 62–73.
- [16] M. Stange, M.E. Dreyer, H.J. Rath, Capillary driven flow in circular cylindrical tubes, Phys. Fluids 15 (2003) 2587–2601.
- [17] N. Fries, Capillary Transport Processes in Porous Materials – Experiment and Model, Cuvillier Verlag Göttingen, 2010.

- [18] M. Dreyer, A. Delgado, H.-J. Path, Capillary rise of liquid between parallel plates under microgravity, *J. Colloid Interface Sci.* 163 (1994) 158–168, <http://dx.doi.org/10.1006/jcis.1994.1092>.
- [19] N. Fries, M. Dreyer, The transition from inertial to viscous flow in capillary rise, *J. Colloid Interface Sci.* 327 (2008) 125–128, <http://dx.doi.org/10.1016/j.jcis.2008.08.018>.
- [20] N. Fries, M. Dreyer, An analytic solution of capillary rise restrained by gravity, *J. Colloid Interface Sci.* 320 (2008) 259–263, <http://dx.doi.org/10.1016/j.jcis.2008.01.009>.
- [21] J. Jurin, An account of some experiments shown before the royal society: With an enquiry into the cause of the ascent and suspension of water in capillary tubes, *Phil. Trans.* 30 (1717) 739–747, (1683–1775).
- [22] D. Quéré, Inertial capillarity, *Europhys. Lett.* 39 (1997) 533–538.
- [23] D. Quéré, E. Raphaël, J.-Y. Ollitrault, Rebounds in a capillary tube, *Langmuir* 15 (1999) 3679–3682, <http://dx.doi.org/10.1021/la9801615>.
- [24] A. Hamraoui, T. Nylander, Analytical approach for the lucas-washburn equation, *J. Colloid Interface Sci.* 250 (2002) 415–421.
- [25] R. Masoodi, E. Languri, A. Ostadhosseini, Dynamics of liquid rise in a vertical capillary tube, *J. Colloid Interface Sci.* 389 (2013) 268–272.
- [26] M. Tani, R. Kawano, K. Kamiya, K. Okumura, Towards combinatorial mixing devices without any pumps by open-capillary channels: fundamentals and applications, *Sci. Rep.* 5 (2015) 10263.
- [27] A. Ponomarenko, D. Quéré, C. Clanet, A universal law for capillary rise in corners, *J. Fluid Mech.* 666 (2011) 146–154, <http://dx.doi.org/10.1017/S0022112010005276>.
- [28] N. Obara, K. Okumura, Imbibition of a textured surface decorated by short pillars with rounded edges, *Phys. Rev. E* 86 (2012) 020601, <http://dx.doi.org/10.1103/PhysRevE.86.020601>.
- [29] C. Ishino, M. Reyssat, E. Reyssat, K. Okumura, D. Quéré, Wicking within forests of micropillars, *Europhys. Lett.* 79 (2007) 56005.
- [30] A. Siebold, M. Nardin, J. Schultz, A. Walliser, M. Oppliger, Effect of dynamic contact angle on capillary rise phenomena, *Colloids Surf. A* 161 (2000) 81–87.
- [31] E.J. LeGrand, W.A. Rense, Data on rate of capillary rise, *J. Appl. Phys.* 16 (1945) 843–846, <http://dx.doi.org/10.1063/1.1707550>.
- [32] R. Siegel, Transient capillary rise in reduced and zero-gravity fields, *J. Appl. Mech.* 28 (1961) 165–170.
- [33] F.G. Wolf, L.O. dos Santos, P.C. Philippi, Capillary rise between parallel plates under dynamic conditions, *J. Colloid Interface Sci.* 344 (2010) 171–179.
- [34] S.J. Liao, *Beyond Perturbation: Introduction to the Homotopy Analysis Method*, CHAPMAN & HALL/CRC, Boca Raton, 2003.
- [35] A. Mastroberardino, Homotopy analysis method applied to electrohydrodynamic flow, *Commun. Nonlinear Sci. Numer. Simul.* 16 (2011) 2730–2736.
- [36] A. Kimiaieifar, E. Lund, O.T. Thomsen, J.D. Sørensen, Application of the homotopy analysis method to determine the analytical limit state functions and reliability index for large deflection of a cantilever beam subjected to static co-planar loading, *Comput. Math. Appl.* 62 (2011) 4646–4655.
- [37] K. Vajravelu, R.A. Van Gorder, *Nonlinear Flow Phenomena and Homotopy Analysis: Fluid Flow and Heat Transfer*, Springer, Heidelberg, 2012.
- [38] J. Sardanyés, C. Rodrigues, C. Januário, N. Martins, G. Gil-Gómez, J. Duarte, Activation of effector immune cells promotes tumor stochastic extinction: A homotopy analysis approach, *Appl. Math. Comput.* 252 (2015) 484–495.
- [39] X.X. Zhong, S.J. Liao, Analytic solutions of Von Kármán plate under arbitrary uniform pressure – equations in integral form, *Sci. China Phys. Mech. Astron.* 61 (2018) 014611.
- [40] S.J. Liao, A new non-perturbative approach in quantum mechanics for time-independent schrodinger equations, *Sci. China Phys. Mech. Astron.* (2019) (doi: 10.1007/s11433-019-9430-4).
- [41] D.L. Xu, Z.L. Lin, S.J. Liao, M. Stiassnie, On the steady-state fully resonant progressive waves in water of finite depth, *J. Fluid Mech.* 710 (2012) 379–418.
- [42] Z. Liu, S.J. Liao, Steady-state resonance of multiple wave interactions in deep water, *J. Fluid Mech.* 742 (2014) 664–700.
- [43] Z. Liu, D.L. Xu, J. Li, T. Peng, A. Alsaedi, S.J. Liao, On the existence of steady-state resonant waves in experiments, *J. Fluid Mech.* 763 (2015) 1–23.
- [44] X. Yang, F. Dias, S. Liao, On the steady-state resonant acoustic-gravitywaves, *J. Fluid Mech.* 849 (2018) 111–135, <http://dx.doi.org/10.1017/jfm.2018.422>.
- [45] X.X. Zhong, S.J. Liao, On the limiting Stokes' wave of extreme height in arbitrary water depth., *J. Fluid Mech.* 843 (2018) 653–679, <http://dx.doi.org/10.1017/jfm.2018.171>.
- [46] A. Hamraoui, K. Thuresson, T. Nylander, V. Yaminsky, Can a dynamic contact angle be understood in terms of a friction coefficient? *J. Colloid Interface Sci.* 226 (2000) 199–204.
- [47] W.A. Rense, Rate of rise of water in capillary tubes, *J. Appl. Phys.* 15 (1944) 436–437.